Nucleotide-dependent farnesyl switch orchestrates polymerization and membrane binding of human guanylate-binding protein 1

Sergii Shydlovskyi[a,1], Anke Y. Zienert[b,1], Semra Ince[a], Christine Dovengerds[a], Annika Hohendahl[c], Julia M. Dargazanli[b], Ailisa Blum[b], Saskia D. Günther[b], Nikolay Kladt[d], Michael Stürzl[e], Astrid C. Schauss[d], Miriam Kutsch[a], Aurélien Roux[c], Gerrit J. K. Praefcke[b,f,2], and Christian Herrmann[a,2]

[a]Physical Chemistry I, Faculty of Chemistry and Biochemistry, Ruhr University Bochum, D-44780 Bochum, Germany; [b]Institute for Genetics, University of Cologne, D-50674 Cologne, Germany; [c]Biochemistry Department, University of Geneva, CH-1211 Geneva, Switzerland; [d]Cologne Excellence Cluster on Cellular Stress Responses in Aging-Associated Diseases, Institute for Genetics, University of Cologne, D-50931 Cologne, Germany; [e]Division of Molecular and Experimental Surgery, Department of Surgery, University Medical Center Erlangen, Friedrich-Alexander University Erlangen-Nürnberg, D-91054 Erlangen, Germany; and [f]Division of Hematology and Transfusion Medicine, Paul-Ehrlich-Institut, D-63225 Langen, Germany

Edited by Peter J. Novick, University of California, San Diego, La Jolla, CA, and approved May 23, 2017 (received for review December 21, 2016)

Dynamin-like proteins (DLPs) mediate various membrane fusion and fission processes within the cell, which often require the polymerization of DLPs. An IFN-inducible family of DLPs, the guanylate-binding proteins (GBPs), is involved in antimicrobial and antiviral responses within the cell. Human guanylate-binding protein 1 (hGBP1), the founding member of GBPs, is also engaged in the regulation of cell adhesion and migration. Here, we show how the GTPase cycle of farnesylated hGBP1 ($hGBP1_F$) regulates its self-assembly and membrane interaction. Using vesicles of various sizes as a lipid bilayer model, we show GTP-dependent membrane binding of $hGBP1_F$. In addition, we demonstrate nucleotide-dependent tethering ability of $hGBP1_F$. Furthermore, we report nucleotide-dependent polymerization of $hGBP1_F$, which competes with membrane binding of the protein. Our results show that $hGBP1_F$ acts as a nucleotide-controlled molecular switch by modulating the accessibility of its farnesyl moiety, which does not require any supportive proteins.

large GTPases | polymerization | membrane tethering | membrane binding | GBPs

Human guanylate-binding protein 1 (hGBP1) is one of seven human guanylate-binding proteins (GBPs) and it is mostly activated in cells after stimulation with type II interferons (IFN-γ) (1). GBPs belong to the dynamin superfamily of large GTPases, also referred to as dynamin-like proteins (DLPs) (2, 3). Among the DLPs the GBPs are most closely related to atlastins, which mediate fusion of endoplasmic reticulum (ER) membranes (4). GBPs have been reported to be involved in the cellular immune responses against bacterial, viral, and protozoan pathogens (5). The antimicrobial function of GBPs has been linked to the ubiquitination and autophagic destruction of pathogen-containing inclusions, inflammasome activation, and the induction of pyroptosis (6, 7). The protein also shows antitumor and antiproliferative (8) effects and has actin remodeling activity (9). However, how the molecular mechanism of GBPs is linked to these diverse functions within the cell remains poorly understood.

In comparison with other DLPs, hGBP1 has a simpler domain architecture: it consists of the large GTPase (LG) domain at the N terminus and an elongated, purely α-helical moiety. The latter is subdivided in the middle domain and the C-terminal α12/13 domain (2, 10, 11). Patches of negatively and positively charged side chains on the LG and α12/13 domains, respectively, are responsible for a tight intramolecular interaction between these domains (12). Upon GTP hydrolysis, this contact is released and structural rearrangements can occur (13, 14).

In contrast to other GTPases, hGBP1 does not only catalyze the hydrolysis of GTP to GDP, but it is also able to catalyze a further phosphate cleavage step leading to the formation of GMP (15, 16). Whereas hGBP1 binds all three guanine nucleotides with similar low affinity (17), GTP binding results in the formation of homodimers of hGBP1 through an interface located on the LG domains (18). Moreover, the protein exhibits concentration-dependent self-activation for catalysis of GTP hydrolysis (11, 19). By formation of an LG domain dimer, an arginine residue is positioned toward the nucleotide pocket leading to enhancement of the catalytic activity (18). Reaction conditions that impair the formation of dimers, e.g., mutations, dilution to low hGBP1 concentrations, or immobilization in a dense packing, result in much slower GTP turnover and in less production of GMP (11, 19–21).

Most members of the dynamin superfamily are involved in processes of membrane reorganization, such as tubulation, fission, and fusion (10). The remodeling of the membrane requires close contact between the protein and the lipid bilayer. In the case of several GBPs, including hGBP1, this is mediated by isoprenylation of a C-terminal CaaX motif, which enables protein's association to the membrane (22–24). HGBP1 itself is isoprenylated with a C15 farnesyl lipid moiety and in addition possesses a polybasic region directly adjacent to the CaaX motif of the protein, which could enhance membrane affinity. We were able to show that farnesylated hGBP1 ($hGBP1_F$) interacts with membranes

Significance

In the human organism, guanylate-binding proteins (GBPs) are involved in antimicrobial and antiviral activity, but the mechanism of GBPs' action remains poorly understood. We have discovered that binding of a substrate molecule, GTP, to the enzyme triggers the release of an aforemasked lipid anchor, which results in GBP polymerization on the one hand and in the attachment of GBPs to lipid membranes on the other. Thus, membrane binding of GBPs competes with protein polymerization and, furthermore, leads to the membrane tethering, which could play a role in a clearance of engulfed pathogens from the cell. Altogether, our findings give deeper insights into GBPs' molecular mechanism in the course of pathogen response.

Author contributions: S.S., A.Y.Z., S.I., C.D., J.M.D., A.R., G.J.K.P., and C.H. designed research; S.S., A.Y.Z., S.I., C.D., A.H., J.M.D., A.B., S.D.G., N.K., M.S., A.C.S., M.K., A.R., G.J.K.P., and C.H. performed research; S.S., A.Y.Z., S.I., C.D., J.M.D., A.B., S.D.G., N.K., A.C.S., A.R., G.J.K.P., and C.H. analyzed data; and S.S., A.Y.Z., S.I., A.R., G.J.K.P., and C.H. wrote the paper.

The authors declare no conflict of interest.

This article is a PNAS Direct Submission.

Freely available online through the PNAS open access option.

[1]S.S. and A.Y.Z. contributed equally to this work.

[2]To whom correspondence may be addressed. Email: chr.herrmann@rub.de or gerrit.praefcke@pei.de.

This article contains supporting information online at www.pnas.org/lookup/suppl/doi:10.1073/pnas.1620959114/-/DCSupplemental.

in the presence of GDP and aluminum fluoride (AlFx), which functions as a mimic of the transition state of GTP hydrolysis (25). In IFN-induced cells, hGBP1 is localized in cytosolic puncta, unidentified to date (26, 27). The addition of AlFx induces redistribution of hGBP1 to the Golgi complex in a farnesylation-dependent manner (26, 28). On the other hand, mutation of the contact between the LG domain and the α12/13 domain results in the localization of hGBP1 at the plasma membrane, whereas a protein mutant impaired in binding nucleotides displays a purely cytosolic staining (12, 27). In the case of murine GBPs, localization to the parasitophorous vacuole of *Toxoplasma gondii* depends on isoprenylation and a functional LG domain (29).

We addressed the mutual regulation of the membrane localization, the nucleotide-dependent oligomerization, and the GTPase activity of hGBP1 by using artificial, protein-free vesicles. Our results reveal that farnesylated hGBP1 can either polymerize into large ordered structures or engage in dynamic interactions with membranes, which results in membrane tethering. Both processes require the transient exposure of the farnesyl moiety to the solvent, which is regulated by GTP binding and GTP hydrolysis. Depletion of GTP or competition with GMP results in the disassembly of hGBP1 polymers and the release from membranes, respectively.

Results

Membrane Binding of hGBP1 Is Farnesylation Dependent and Nucleotide Controlled. To observe the interaction of hGBP1 with membranes in real time, we investigated the behavior of $hGBP1_F$ and non-farnesylated hGBP1 ($hGBP1_{NF}$) in the presence of giant unilamellar vesicles (GUVs, 5–50 μm). GUVs were prepared from brain polar lipid (BPL) extract to represent membranes of the phagolysosomal pathway. First, we checked how the binding of different nucleotides might influence the interaction between $hGBP1_F$ and vesicles. Therefore, tetramethyl rhodamine-labeled GUVs were incubated with 2.5 μM Alexa Fluor 488-labeled $hGBP1_F$ ($AF\text{-}hGBP1_F$) either in the absence of nucleotide (apo state) or in the presence of GMP, GDP, or the GTP analogs, GppNHp or GTPγS. No sign of $AF\text{-}hGBP1_F$ binding to GUVs was observed in the absence of nucleotide and in the presence of either GMP or GDP (Fig. 1 *A* and *C*). However, in the presence of GppNHp, a faint protein fluorescence was detectable on the surface of the GUVs (Fig. 1 *A* and *C*). Moreover, the presence of GTPγS led to a strong homogenous stain of $AF\text{-}hGBP1_F$ on the surface of GUVs, indicating that hGBP1 binding to membranes occurs in a GTP-dependent fashion (Fig. 1 *A* and *C*). In contrast, $AF\text{-}hGBP1_{NF}$ revealed no binding to GUVs—neither in the apo state nor in the presence of GTPγS (Fig. 1 *B* and *C*).

To study the association of $AF\text{-}hGBP1_F$ with GUVs in the presence of the genuine substrate, we performed a similar set of experiments with GTP at its initial concentration of 1 mM. Due to the ability of hGBP1 to hydrolyze GTP rapidly, we followed the binding of $AF\text{-}hGBP1_F$ to GUVs over time. These experiments yielded initial binding of $AF\text{-}hGBP1_F$ to GUVs, which decayed over time due to depletion of GTP (Fig. 1 *D* and *E*). The decay was not due to photobleaching, as we used an oxygen scavenging solution in these experiments (*Methods*). Toward the end of each experiment (i.e., after 15–20 min) protein fluorescence was hardly detectable on the surface of GUVs and the background signal representing free $AF\text{-}hGBP1_F$ increased (Fig. 1*D*). We also observed the same behavior of $AF\text{-}hGBP1_F$ binding to GUVs in the presence of GTP when we monitored a pool of GUVs instead of a single vesicle (Fig. S1*A*). In this case, we disclosed different patterns of protein distribution on the membrane surface but altogether more than 70% of the total vesicle surface was covered by a faint, homogeneous stain, most likely representing a monolayer of $AF\text{-}hGBP1_F$ (Fig. S1 *B* and *C–F*).

In addition to wild-type protein, we investigated GTPase-deficient and GDPase-deficient mutants of hGBP1 having R48A

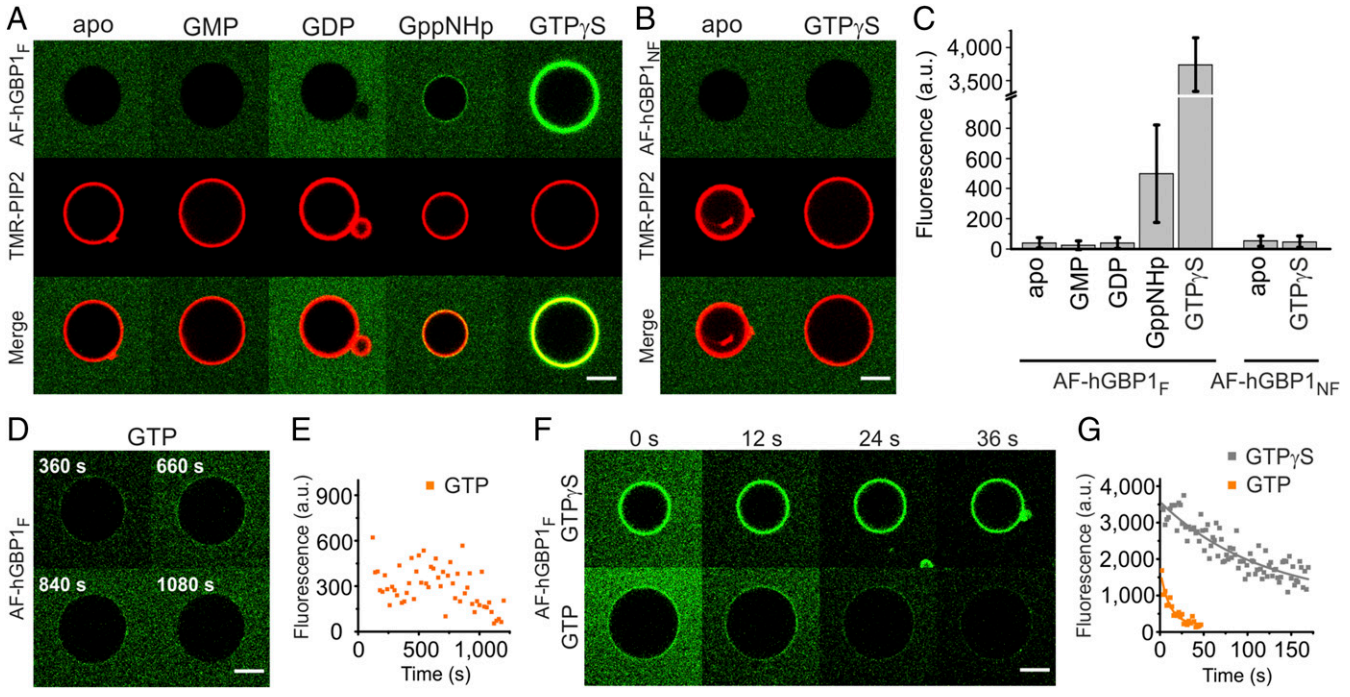

Fig. 1. Interaction of hGBP1 with GUVs. (*A*) GUVs labeled with 1% TMR-PIP_2 (red) in the presence of 2.5 μM $AF\text{-}hGBP1_F$ (green) and 400 μM corresponding nucleotides after 5 min of incubation. (*B*) Same as in *A*, but in the presence of $AF\text{-}hGBP1_{NF}$. (*C*) Mean fluorescence intensities of AF-hGBP1 binding to GUVs (*Methods*) for different nucleotides. Statistics include the data for $n = 25$–80 GUVs under each experimental condition from at least two independent measurements. (*D*) Time-dependent dissociation of $hGBP1_F$ from a GUV in the presence of GTP monitored on a single vesicle. The experiment was started by addition of 1 mM GTP ($t = 0$ s) into a solution containing 2.5 μM $AF\text{-}hGBP1_F$. (*E*) Numerical representation of *D*. (*F*) Time-lapse images of $AF\text{-}hGBP1_F$ dissociation from GUVs in the presence of 400 μM GTPγS (*Upper*) or 400 μM GTP (*Lower*) (see also Movie S1). (*G*) Numerical representation of *F*. (Scale bars, 5 μm.) a.u., arbitrary units.

and K76A mutations (30), respectively, for their ability of membrane association with GUV-binding setup. Both Alexa-fluorescent R48A and K76A farnesylated mutants (AF-R48A$_F$ and AF-K76A$_F$, respectively) bound to GUVs in the presence GTPγS and GTP, which was not the case in the absence of the nucleotide (Fig. S2*A*). Intriguingly, the degree of binding to GUVs of AF-R48A$_F$ in the presence of GTP was comparable to the presence of GTPγS, which was not the case for AF-hGBP1$_F$ and AF-K76A$_F$ (Fig. S2*A*).

In the previous experiments, GTP and AF-hGBP1$_F$ were mixed in a reaction tube before the mixture was transferred into the chamber. To see what happens directly after mixing the protein and GTP, we modified the previous experimental setup such that GTP was added into the chamber as a droplet only after AF-hGBP1$_F$ and GUVs were already preincubated. Under these experimental conditions, nucleotide spread in the chamber by diffusion. While recording a single GUV, we instantly observed binding of AF-hGBP1$_F$ comparable to the first experiment, which was followed by a sudden drop of the background fluorescence. Concomitantly, floating protein clusters became visible, suggesting that hGBP1$_F$ may be able to form polymers (Fig. S1*G*).

In the assay described above, the system remained at equilibrium conditions and it is difficult to conclude anything about the kinetics of the protein interaction with GUVs. To investigate the kinetics of AF-hGBP1$_F$ dissociation from GUVs, we performed an assay at nonequilibrium conditions. GUVs were incubated in the chamber with either GTP or GTPγS, and further, a short local injection of AF-hGBP1$_F$ into the vicinity of observed GUVs was performed from the injection pipette, containing 90 μM of protein. The presence of the corresponding nucleotide in the chamber resulted in instant binding of AF-hGBP1$_F$ to GUVs. Due to diffusion, the protein concentration in the vicinity of the observed GUV decreased, leading to dissociation of AF-hGBP1$_F$ from the GUV's surface (Fig. 1*F*). Remarkably, AF-hGBP1$_F$ dissociation from GUVs occurred much faster in the presence of GTP compared with GTPγS (Fig. 1 *F* and *G* and Movie S1). Single exponential decays fitted to the recorded fluorescence of AF-hGBP1$_F$ on the GUVs (Fig. 1*G*) yielded observed rate constants (k_{obs}) for dissociation of AF-hGBP1$_F$ from the membrane with values of 0.082 s^{-1} and 0.006 s^{-1} for experiments in the presence of GTP and GTPγS, respectively. Compared with Fig. 1 *D* and *E*, the decays were much faster, as they reflect predominantly the dissociation of the protein because reassociation was suppressed by the rapid diffusion of dissociated hGBP1 away from the GUV.

The comparison of GTP and GTPγS reveals a more than 10-fold faster dissociation rate of AF-hGBP1$_F$ from the surface of GUVs in the presence of GTP compared with its analog. It may be explained by the GTPase activity of AF-hGBP1$_F$, involving structural changes including the C-terminal moiety. Of note, the very slow turnover of GTPγS bound to hGBP1$_F$ is 0.0001 s^{-1} (Fig. S3*E*), i.e., the membrane dissociation mentioned above is 60-fold faster. With the above-described dissociation assay, we also challenged farnesylated R48A, which showed almost no GTPase activity (Fig. S2*C*). Dissociation experiments with AF-R48A$_F$ revealed similar dissociation rates for the experiments performed with GTP and GTPγS (Movie S1), yielding dissociation rate constants of 0.012 s^{-1} and 0.014 s^{-1}, respectively. These values are comparable to the wild-type protein in the presence of GTPγS, underlining the importance of GTPase activity for membrane dissociation.

We used an independent FRET-based experimental setup to demonstrate nucleotide-dependent membrane binding of hGBP1$_F$, in which we used large unilamellar vesicles (LUVs) of various sizes. LUVs, labeled with Rhodamine-PE lipids acting as acceptor fluorophore, were mixed with Alexa-488 labeled Q577C mutant of hGBP1 (AF-Q577C$_F$) acting as donor fluorophore. After addition of GTPγS, the FRET efficiency increased reporting attachment of hGBP1$_F$ to the membrane. Moreover, the fluorescence value returned to its initial value after addition of a large molar excess of GMP (Fig. S3*A*). As nucleotide exchange is rapid (Fig. S3*D*), this finding is interpreted as dissociation of GMP-bound hGBP1$_F$ from the membrane with a rate constant of 0.003 s^{-1} (Fig. S3*A*). Intriguingly, both the increase of fluorescence and the dissociation rate are the same for small and large LUV diameters, respectively (Fig. S3*A*). With the same setting, the addition of GppNHp yielded a smaller and slower increase of fluorescence, whereas the addition of GDP led to only a very small jumpwise increase of fluorescence (Fig. S3*B*).

Electron Microscopy Analysis of hGBP1$_F$. To gain insight into the architecture of the protein clusters formed by hGBP1$_F$ (Fig. S1*G*), we used negative stain electron microscopy (EM). In the presence of GTP, we observed a large number of circular structures with diameters around 60 nm (Fig. 2, orange arrows). The centers of these rings were always formed by a light dot. Besides these circular structures, we also observed some elongated structures of variable length between 60 nm and more than 200 nm and a width of about 50 nm (Fig. 2, white arrowheads). Circular structures with a white dot in the center and of a similar diameter were also observed for hGBP1$_F$ in the presence of GDP·AlFx. However, these GDP·AlFx-induced circular structures were lower in number than those observed in the presence of GTP (Fig. 2, orange arrows). Moreover, the elongated structures as observed with the natural substrate GTP were not formed in the presence of GDP·AlFx. Instead, we observed a large number of rod-like structures with a length of about 50 nm and a width of about 20 nm (Fig. 2, white arrows). These rods having a length similar to the ring diameter may therefore represent the same objects as the circular structures viewed from a different angle, in particular from the side view. Notably, the analog GTPγS did not induce any structured arrangement of hGBP1$_F$ at all (Fig. S4*A*), and

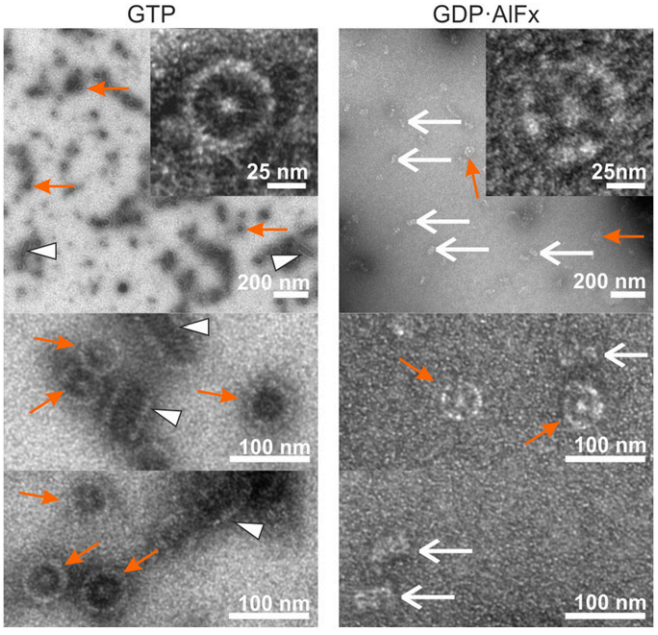

Fig. 2. EM images of hGBP1. Representative images of hGBP1$_F$ in the presence of GTP or GDP·AlFx. Experimental mixture contained 10 μM of hGBP1$_F$ and 1 mM of GTP or 200 μM GDP, 300 μM $AlCl_3$, and 10 mM NaF for samples with GDP·AlFx. Reactions were stopped after ∼10 min of incubation with GTP and after ∼20 min incubation with GDP·AlFx (*Methods*). Ordered polymer structures of hGBP1$_F$ in the presence of GTP or GDP·AlFx were identified during at least three independent measurements. Examples of observed ring-like structures are indicated with orange arrows, rods with white arrows, and elongated structures with white arrowheads. Scale bars are as indicated. The geometries of all identified polymer structures are quantified in Fig. S4*B*.

$hGBP1_{NF}$ also did not yield any clusters irrespective of the nucleotide used (Fig. S4*A*). In summary, these data demonstrate that farnesylated hGBP1 is capable of forming polymeric structures in a nucleotide-dependent manner.

Farnesylated hGBP1 Undergoes GTP-Dependent Reversible Polymerization. To further investigate the polymerization of $hGBP1_F$, we followed the absorbance of protein samples at 350 nm upon injection of different nucleotides, which enabled us to detect turbidity as an indicator for polymerization of the protein. Injection of GTP induced a strong increase in turbidity of the $hGBP1_F$ solution, whereas this was not the case for $hGBP1_{NF}$ (Fig. 3*A* and Fig. S5*B*). Remarkably, turbidity appeared with a delay, peaked a few minutes after injection of GTP, and then decreased back to the baseline (Fig. 3*A*). The kinetics as well as the extent of $hGBP1_F$ polymerization depended on the protein concentration (Fig. S5*A*). The disappearance of turbidity was due to the complete dissolution of the polymers and not due to the sedimentation of large aggregates. This result was demonstrated by rapid centrifugation of samples taken (*i*) immediately after addition of GTP, (*ii*) at the time of peaking turbidity, and (*iii*) after turbidity had almost vanished and analysis by SDS/PAGE. Only for the second sample, hGBP1 was found in the pellet fraction but not for the first and the third samples (Fig. S5*E*). Using $hGBP1_F$, the addition of GMP, GDP, or GTPγS did not trigger any polymerization of the protein (Fig. 3*A*). The addition of GDP·AlFx to $hGBP1_F$ revealed only a modest polymerization, which was not reversible (Fig. 3*A*). These observations are in good agreement with dynamic light scattering (DLS) experiments for $hGBP1_F$ and $hGBP1_{NF}$. DLS experiments indicated reversible transient appearance of large polymers of $hGBP1_F$ in the presence of GTP hydrolysis and nonreversible appearance of relatively small polymers in the presence of GDP·AlFx (Fig. S5*C*) with an apparent hydrodynamic radius of about 30 nm, which corresponds reasonably well with the structures seen in the EM. Human $GBP1_{NF}$ was not able to polymerize at all, neither in the presence of GTP nor in the presence of GDP·AlFx (Fig. S5 *B* and *D*).

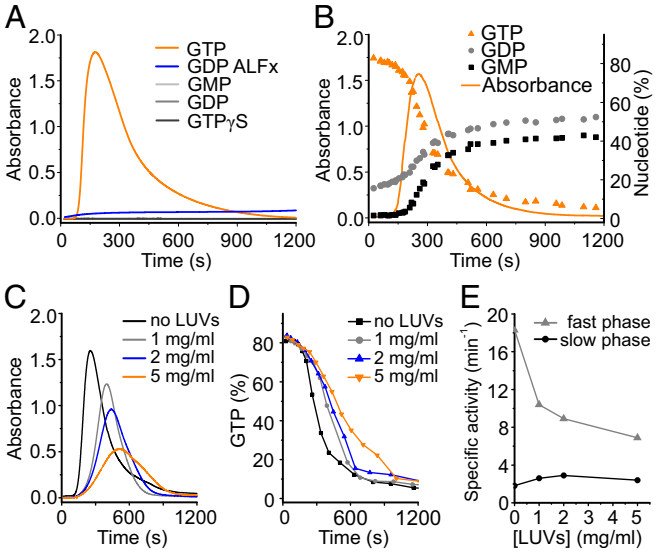

Fig. 3. Regulation of GTPase activity of $hGBP1_F$ by polymerization and membrane interaction. (*A*) Absorbance signal of 10 μM $hGBP1_F$ after injection of nucleotides at $t = 0$ s. (*B*) Absorbance signal of 10 μM $hGBP1_F$ after injection of 1 mM GTP ($t = 0$ s) superimposed with nucleotide composition in the same solution. The plot includes data from three independent experiments; absorbance represents the average of all three datasets. (*C*) Absorbance signal of 10 μM $hGBP1_F$ after injection of 1 mM GTP in the presence of different concentrations of LUVs. The baseline of LUVs alone was subtracted from the raw data (Fig. S6 *A* and *B*). (*D*) GTP turnover from experiments described in *C*. (*E*) Enzymatic activity of 10 μM $hGBP1_F$ in the presence of different LUV concentrations. Specific activities of GTP hydrolysis in the slow and fast phases were calculated from the data presented in *D*.

To understand the link between polymerization of $hGBP1_F$ and its GTPase activity, we simultaneously measured the absorbance and analyzed the nucleotide composition in the same cuvette containing 10 μM $hGBP1_F$ after addition of 1 mM GTP (Fig. 3*B*). We observed a biphasic profile of GTPase activity of $hGBP1_F$ comprising an initial slow phase with a turnover number of 1.6 $min^{-1} \pm 0.6$ min^{-1} followed by a fast phase with a turnover number of 15.8 $min^{-1} \pm 0.7$ min^{-1}. As could be seen from Fig. 3*B*, this acceleration of the catalytic hydrolysis reaction nicely correlated with the appearance of the turbidity. Moreover, there was an obvious delay in GMP production in the course of the experiment and the onset of GMP production coincided with the onset of turbidity as well as with the change from the slower to the faster turnover rate. We also checked the ability of $R48A_F$ and $K76A_F$ mutants of hGBP1 to polymerize using the turbidity assay. Intriguingly, both mutants did not show any increase of turbidity after mixing with GTP (Fig. S2*B*). As mentioned already, $R48A_F$ showed almost no GTPase activity. $K76A_F$ showed a reduced activity of GTP hydrolysis and almost no activity for the second step leading to GMP formation (Fig. S2 *C*–*E*).

We further questioned how the presence of liposomes alters the polymerization and GTPase activity of $hGBP1_F$. To answer this question, we performed similar experiments in the presence of different concentrations of LUVs. Increasing amounts of LUVs resulted in a delayed and less pronounced polymerization of $hGBP1_F$ (Fig. 3*C* and Fig. S6*A*). Moreover, the presence of LUVs did not affect the first slow phase but did affect the second fast phase of GTP hydrolysis in two ways: with increasing LUV concentration, not only GTPase activity (Fig. 3 *D* and *E*) but also GMP formation decreased (Fig. S6*D*). Biphasic behavior of GTPase activity of $hGBP1_F$ was pronounced most remarkably at 25 °C, even for reduced protein concentrations (Fig. S6*E*). Nevertheless, at 37 °C this biphasic behavior could also be recognized in the absence of LUVs, and the presence of LUVs elongated the slow phase of enzymatic activity (Fig. S6*F*). In contrast, we did not observe biphasic behavior of catalytic activity for $hGBP1_{NF}$, neither at 25 °C, nor at 37 °C (Fig. S6 *G* and *H*). The presence of LUVs did not alter the GTPase activity of $hGBP1_{NF}$ at either temperature (Fig. S6 *G* and *H*).

Having shown both GTP-dependent GUV binding and polymerization of $hGBP1_F$, we used the FRET-based LUV binding assay described above. After addition of GTP to the mixture of LUVs and $AF\text{-}Q577C_F$ first, an increase of fluorescence intensity was observed which then changed to a decrease and after a few minutes came back to the initial value. This observation can be explained by rapid membrane attachment followed by polymerization of $hGBP1_F$, which leads to decreased fluorescence intensity likely due to turbidity (Fig. S3*C*). Finally, after GTP is depleted, the initial situation of dissociated $hGBP1_F$ is reestablished; all this happened on time scales as observed in the turbidity assay reporting polymerization as shown in Fig. 3*C*.

Membrane-Bound hGBP1 Tethers GUVs in a Nucleotide-Dependent Manner. During GUV-binding experiments with $AF\text{-}hGBP1_F$, we observed that GUVs spontaneously contacted each other. Notably, the contact area between those GUVs was larger in the presence of GTPγS compared with other nucleotides. To get insights into this phenomenon, we performed the following tethering assay: pairs of GUVs were gently brought into contact with each other in the presence of 22.5 μM of $hGBP1_F$ containing 11 mol% of $AF\text{-}hGBP1_F$. Further, with the help of an injection pipette containing 400 μM of either GTPγS or GTP, the nucleotide was briefly injected (within 5–10 s) into the vicinity of the

observed pair of GUVs. This event and subsequent rearrangements of the given GUV pair were tracked with confocal microscopy. Although the contact area gives the true measure for tethering, here, we exploited the contact length from confocal microscopy images instead (Fig. S7*E* and *SI Methods*), considering that an increase of the contact length implicates an increase of the contact area. Additionally to the contact length, we also quantified the fluorescence of membrane-bound protein for a given pair of GUVs.

Strikingly, in the course of such experiments we noticed a different behavior for GTPγS compared with GTP. Upon injection of GTPγS we observed irreversible binding of AF-hGBP1$_F$ to GUVs and a nonreversible tethering effect of GUV pairs on a time scale of several minutes. After initial injection of the nucleotide, the contact length between pairs of GUVs increased until the maximum value was reached (Fig. 4*A* and Movie S2). In contrast, the binding of AF-hGBP1$_F$ and the tethering effect on GUVs was reversible upon injection of GTP and could be repeated several times for one pair of GUVs (Fig. 4*B* and Movie S3). Importantly, the change of the contact length between a given pair of GUVs correlated with the fluorescence signal of GUV-bound AF-hGBP1$_F$ resulting in a more dynamic system when the natural substrate GTP was supplied instead of the analog GTPγS (Fig. 4 *A* and *B*). As a control, tethering experiments with hGBP1$_{NF}$ did not reveal any binding of the protein or any increase of the contact length upon injection of GTPγS (Fig. 4*C* and Movie S4). The same was observed for hGBP1$_{NF}$ and injection of GTP (Movie S5). Generally, for experiments with hGBP1$_{NF}$, GUVs that were initially brought into contact with each other had a tendency to separate from each other, rather than to adhere, upon injection of the nucleotide.

The notion that hGBP1$_F$ tethers vesicles in a GTP-dependent manner is supported by two additional experiments, as similarly performed on atlastin (31), which do not rely on initial contacting of the vesicles. First, LUVs of various sizes in the presence of hGBP1$_F$ showed an increase of turbidity after addition of GTPγS, which was not the case after addition of GMP, GDP, GppNHp, or when hGBP1$_{NF}$ was used instead (Fig. S8*A*). Moreover, the GTPγS-induced increase of turbidity was driven back by the addition of a large molar excess of GMP, which could be explained by disassembly of tethered vesicles (Fig. S8*A*). Second, green fluorescent LUVs and red fluorescent LUVs were mixed, showing separate spots under the microscope. After addition of GTPγS, the green and red spots disappeared as they merged, yielding yellow spots indicating colocalization, which we interpret as LUV tethering (Fig. S8*B*). Again, the addition of GMP could reverse this effect, leading to separate green and red spots. This is documented together with further control experiments in Fig. S8. There we show also weaker tethering mediated by the R48A variant in the presence of GTP and GTPγS, respectively (Fig. S8*C*).

HGBP1 Reveals Fast Membrane Dynamic in Cells. To compare the in vitro membrane dynamics to experiments in living cells we analyzed the recruitment of hGBP1 to cellular membranes in HeLa cells. In previous studies IFNγ-induced endogenous hGBP1 has been found in a punctate or vesicular cytoplasmic distribution throughout the whole cell (27). However, the exact assignment of the punctate structures to an intracellular membranous compartment has not been made. To probe for a phagolysosomal localization of hGBP1, we incubated IFNγ-induced HeLa cells with latex beads to induce phagocytosis (Fig. S9). Endogenous hGBP1 was recruited to these phagocytosed beads, although it was often not equally distributed around the entire beads but present in punctate structures. HGBP1 partially colocalized with marker proteins of the phagolysosomal pathway such as early endosomes (Rab5 and EEA1), late endosomes (Rab7), and lysosomes (LAMP1). These hGBP1$^+$ puncta also colocalized with

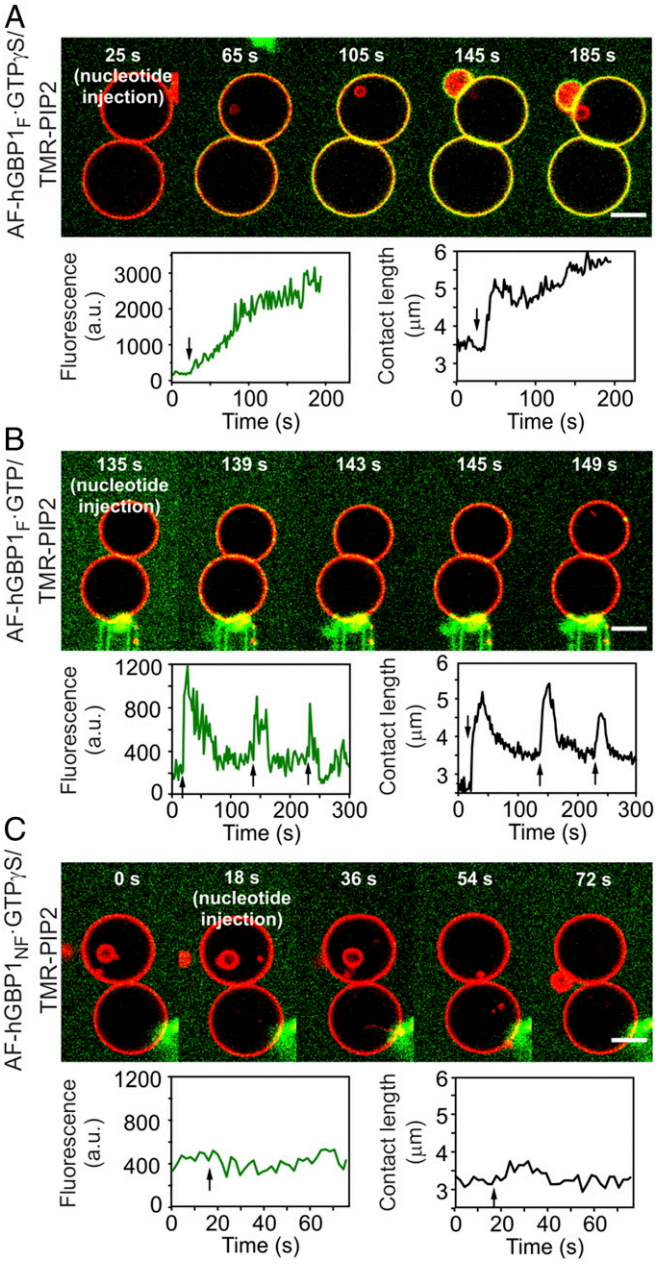

Fig. 4. Tethering experiments on pairs of GUVs. (*A*) Time-lapse confocal images of GUV pairs (red) in the presence of hGBP1$_F$ (green) and GTPγS (*Top*) (see also Movie S2). Images were analyzed with respect to the fluorescence signal of the protein on the membrane of GUVs (*Bottom Left*) and contact length between a pair of GUVs (*Bottom Right*). Experiments were performed in the presence of 2.5 μM of labeled and 20 μM of nonlabeled protein. Arrows indicate time points of nucleotide injections. (*B*) Same as in *A* but with GTP (see also Movie S3). (*C*) Same as in *A* but with hGBP1$_{NF}$ (see also Movie S4). (Scale bars, 5 μm.) a.u., arbitrary units.

filamentous actin stained with fluorescently labeled phalloidin enclosing a phagocytosed bead.

Similar events were observed upon transfection of unstimulated HeLa cells with fluorescent protein-tagged hGBP1 and marker proteins (Fig. S10). Recombinant mCherry-hGBP1 colocalized with GFP-Rab5, GFP-Rab7, GFP-Rab9, or LAMP1-GFP around bead-containing phagosomes (Fig. S10 and Movie S6). The colocalization of mCherry-hGBP1 with Rab$^+$ vesicular structures was enhanced compared with untransfected cells.

The dynamics of hGBP1 on cytosolic punctate structures and on bead-containing phagosomes (BCP) were determined by fluorescence recovery after photobleaching (FRAP). Before imaging, unstimulated HeLa cells cotransfected with mCherry-hGBP1 and GFP-tagged Rab7 were incubated with latex beads. After bleaching of a region of interest (ROI), the fluorescence bleached on BCPs or late endosomes positive for mCherry-hGBP1 and GFP-Rab7 recovered in all cases but usually not to the starting value. An exemplary time lapse for the recovery of mCherry-hGBP1 and GFP-Rab7 fluorescence on a vesicular structure is shown in Fig. 5. The signal for fluorescence of mCherry-hGBP1 reappeared quickly within 2 s, whereas the first faint GFP-Rab7 signal could only be detected after 20 s. It is striking that the overall fluorescence within the depicted cell decreased after bleaching of the ROI, which is most probably due to the long exposure with a high laser power and indicates a relatively fast exchange of the fluorescent components with the surrounding cytosol. Consequently, to normalize the data, an ROI was set outside of the observed cell additionally to the one in an unbleached cytoplasmic area inside the cell.

Mean values of fluorescence recovery half-lives ($\tau_{1/2}$) are indicated in Fig. 5 *B* and *C*. On punctate vesicular structures, the signal for mCherry-hGBP1 recovers within a few seconds, which is significantly faster than the signal of GFP-Rab7, which recovers with a similar $\tau_{1/2}$ values in the range of 10–50 s as previously reported for human melanoma cells (32). On BCPs, the recovery of hGBP1 is slower and more variable and resembles that of GFP-Rab7. Because the entire vesicular structures or BCPs were bleached in each experiment, recovery of fluorescence could only be achieved by de novo delivery of fluorescent protein-tagged hGBP1 or Rab7 molecules, entering the bleached area from the surrounding parts of the cell and not by lateral diffusion. This indicates a very fast exchange of material between the membrane-bound pool of hGBP1 and the cytosol. In line with this notion is the finding that the fluorescence never recovered to more than 80% of the prebleach values, which can be explained by the long time needed to completely bleach the entire structures.

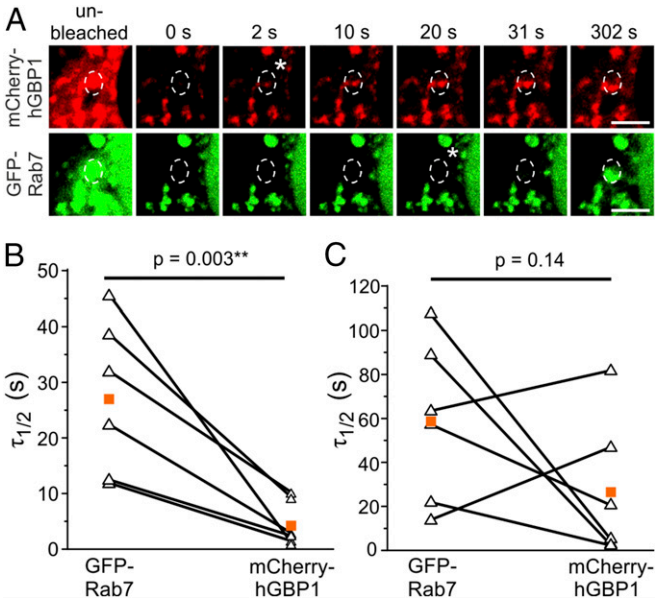

Fig. 5. Fast recovery of mCherry-hGBP1 on GFP-Rab7$^+$ structures. (*A*) FRAP: time lapse of mCherry-hGBP1 and GFP-Rab7 fluorescence recovery on a vesicle in cotransfected HeLa cells after bleaching. The first picture of each panel shows the region of interest (dashed circle) before bleaching. Asterisks mark first detection of recovering signals. (Scale bars, 10 μm.) (*B* and *C*) Data plots showing the half-lives of fluorescence recovery ($\tau_{1/2}$) of cotransfected mCherry-hGBP1 and GFP-Rab7 on vesicular structures (*B*) and BCP signals (*C*) after photobleaching. Values obtained for both protein constructs in the same measurement are connected by lines. Orange squares indicate the mean values.

Discussion

The guanylate-binding proteins function in innate immunity against bacteria, viruses, and protozoan pathogens (5–7). Furthermore, they are involved in the regulation of proliferation and migration of endothelial cells (8). For both functions, the ability to interact with cellular membranes is a prerequisite. In the case of hGBP1 and murine GBP2 (mGBP2), abolishing the C-terminal lipid modification results in biologically inactive proteins (26–28, 33). To understand the function and mechanism of hGBP1 on a molecular level, it is therefore of critical importance to study the protein in the lipid modified state.

Using GUVs and LUVs, we were able to study the binding of fluorescently labeled and farnesylated hGBP1 in real time, in particular in the presence of GTP. Most intriguingly, $hGBP1_F$ associated with membranes only in the presence of either GTP or its nonhydrolyzable analog GTPγS, but not in the absence of nucleotide or when the GTP hydrolysis products GDP or GMP were added (Fig. 1 and Fig. S3). Nonfarnesylated hGBP1 was not able to associate with GUVs, irrespective of the nucleotide supplied (Fig. 1*B*). The rate of association of $hGBP1_F$ to GUVs after addition of GTP occurs rapidly; most probably it is controlled by the rate of mixing and cannot be resolved accurately with these assays. The rate of $hGBP1_F$ dissociation from the GUV membrane could be defined more accurately: the dissociation of GTPγS-bound $hGBP1_F$ from GUVs occurred with a half-life of about 120 s. In the case of GTP-bound $hGBP1_F$, the residence time is about 10 s, which is similar to the reciprocal rate constant of hGBP1-catalyzed GTP hydrolysis when bound to the membrane. Because the diffusion of a protein in the cytosol over a distance of a few micrometers is faster than a second, the dynamics of hGBP1 intermembrane traveling are most likely to occur in the range of 10 s, controlled by the rate of dissociation from the membrane. Our data suggest that GTP hydrolysis boosts dissociation of $hGBP1_F$ from the membrane. However, we have previously demonstrated the ability of $hGBP1_F$ to associate with liposomes only in the presence of GDP·AlFx but not in the presence of GTP (25). This disagreement to the present data is probably due to the dynamics of the membrane interaction of GTP-bound $hGBP1_F$, which impairs the detection in a liposome cosedimentation assay. From our current study, we conclude that GTP binding is sufficient to trigger association of $hGBP1_F$ to the membrane and GTP hydrolysis is not required for that. Moreover, membrane binding of $hGBP1_F$ seems to not be sensitive to the membrane curvature as the assayed liposomes covered a wide range of diameter from 0.1 μm to 10 μm and did not show considerable differences in binding.

For other proteins carrying a membrane anchor like farnesyl, geranylgeranyl, palmitoyl, or myristoyl groups, in particular GTP-binding proteins, it is well known that their membrane localization is not permanent but rather dynamic, allowing the proteins to translocate to different membranes or even to the cytosol (34). Many examples of Ras-like proteins show nucleotide-dependent shuttling between various membrane compartments, e.g., the GTP-binding and hydrolysis-driven function of Rab proteins is the traveling between organelles and thereby directing the transport of cargo. These cycles of membrane binding and dissociation are facilitated by specific helper proteins [guanine-nucleotide dissociation inhibitors (GDIs)], which take up the isoprenyl anchor in a binding pocket to enable the GTP-binding protein to leave the membrane and travel through the cytosol (35). This mechanism is crucially different for hGBP1 and resembles that of N-terminally myristoylated Arf proteins (36). Human $GBP1_F$ attaches to the membrane upon GTP binding and leaves the membrane as a

soluble protein when no more GTP is available, obviously not requiring any helper protein for positioning its farnesyl anchor inaccessible for other interaction partners (like the membrane) as is the case for small Ras-like Rho and Rab GTPases (35). Thus, we report that the accessibility of an isoprenyl anchor from a GTP-binding protein is exclusively controlled by the associated nucleotide. We term this mechanism nucleotide-dependent farnesyl switch of hGBP1.

In addition to farnesyl- and nucleotide-dependent membrane binding, we discovered the ability of farnesylated hGBP1 to polymerize in a GTP-dependent manner. Human $GBP1_F$ polymerized reversibly in the presence of GTP and irreversibly in the presence of GDP·AlFx. However, in the presence of GDP·AlFx, $hGBP1_F$ formed polymers to a much lower extent compared with GTP (Fig. 3). Despite the structural changes within the protein, which occur upon binding of GTPγS and which lead to the accessibility of the farnesyl moiety, binding of this nucleotide does not result in polymerization of $hGBP1_F$ as inferred from turbidity as well as from electron microscopy experiments (Fig. 2 and Fig. S4*A*). We suggest that only GTP hydrolysis is able to mediate conformational changes within the protein structure, which are sufficient for the assembly of $hGBP1_F$ and likely multiple rounds of GTP turnover are needed for efficient polymer formation. Considering the biphasic behavior of enzymatic activity, during the first slow phase (1.6 min^{-1}) five GTP molecules can be estimated to be hydrolyzed per enzyme molecule but the second cleavage step resulting in GMP does not occur here. The second phase shows a roughly 10 times faster turnover of GTP, and additionally, the second cleavage step is observed yielding GMP. This biphasic behavior of $hGBP1_F$ is more pronounced at 25 °C but also present at 37 °C and has not been observed for nonfarnesylated hGBP1 (19) (Fig. S6), suggesting a principal difference between the way of action of farnesylated and nonfarnesylated hGBP1. The rate of the fast phase of $hGBP1_F$ is similar to the self-stimulated enzymatic activity of nonfarnesylated hGBP1 that is achieved by LG domain interactions at sufficiently high protein concentration. Also, the product ratio of GDP and GMP under these conditions for nonfarnesylated hGBP1 resembles the GDP/GMP ratio produced by farnesylated hGBP1 in this phase. In contrast, the slow phase of $hGBP1_F$ does not lead to detectable GMP production, similar to the observation with nonfarnesylated hGBP1 at low concentrations, where self-activation is not possible (16, 18). Furthermore, the observed onset of turbidity, accompanied by the change from slow to fast mode of $hGBP1_F$ activity, corresponds to a time of about five cycles of GTP hydrolysis in the slow phase. The strong but fully reversible polymerization of $hGBP1_F$ during GTP hydrolysis is highly reminiscent of the transient polymerization of murine Irga6 (37). The mutants R48A and K76A of $hGBP1_F$, respectively, show no polymerization in the presence of GTP, underlining the importance of enzymatic activity (Fig. S2). Whereas R48A is almost completely impaired in GTPase activity, K76A showed a four- to fivefold reduced GTPase activity compared with the slow phase of wild type and almost no GMP production. As for this mutant, the second cleavage step is blocked but also the first step is slower than for the wild type; unfortunately, we cannot safely conclude as to the importance of the first and second cleavage steps for polymer formation. The absence of polymer formation of the K76A mutant can be due to the impaired second cleavage step of the nucleotide but it may also be explained by the smaller rate of the first step. For addressing the role of the second hydrolysis step within polymerization, we also considered GpCpp as a suitable GTP analog. However, $hGBP1_F$ did not bind GpCpp (Fig. S3*F*).

We have observed circular polymer structures of $hGBP1_F$ with a diameter of about 60 nm in the presence of both GTP and GDP·AlFx (Fig. 2). Similar ring-like structures have been reported for dynamin, human MxA, *Dictyostelium discoideum* dynamin *A* (DymA) in the absence of lipids (38–40), and for bacterial dynamin-like protein (BDLP) in the presence of lipids (41). DLPs involved in fission reaction can assemble into helical polymers even in the absence of nucleotides. In the case of $hGBP1_F$, however, the circular structures are formed in the absence of lipids and in the presence of GDP·AlFx or GTP. The radius of these structures is strikingly similar to the hydrodynamic radius of $hGBP1_F$ in the presence of GDP·AlFx, observed by DLS and to the length of about 30 nm—a length that also applies to an $hGBP1_F$ molecule in a completely open and stretched conformation of the α12/13 domain. In this conformation, the $hGBP1_F$ molecule resembles a cone-like geometry. These observations and the analogy to other DLPs support our model shown in Fig. 6, where the LG domains reside outside and the farnesyl anchors in the center. With a width of about 4–5 nm for the LG domain, a full turn of the ring would comprise about 40–50 GBP molecules. Larger oligomers, which are observed only for GTP, may represent helices or stacks of circular structures leading to the elongated structures in Fig. 2.

Based on previous reports that nonfarnesylated hGBP1 undergoes major intramolecular opening and particularly releases the α12/13 domain upon GTP binding (12–14), we suggest that also farnesylated protein after mixing with GTP opens up in a similar way, thereby releasing the farnesyl anchor, which leads to polymerization of $hGBP1_F$ in an along-side orientation during the first phase. At the end of the first phase, this results in circular structures of the polymers with the farnesyl groups facing the center of the polymer and with the LG domain of the enzyme pointing outward as indicated in our model (Fig. 6). Up to this point, the LG domains do not form GTPase activating contacts to each other and hence provide only a low enzymatic activity. Now, with the change from the first to the second phase, we suggest that the circular structures grow or associate with each other stackwise, to form elongated, cylindrical structures becoming visible by turbidity. At the same time, the LG domain

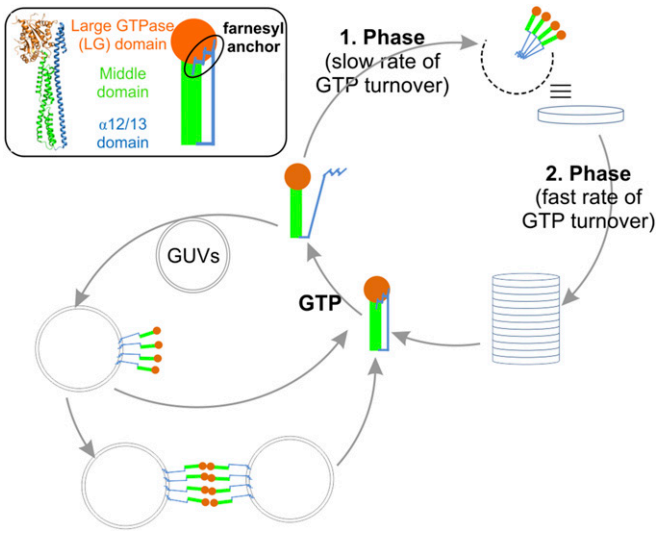

Fig. 6. Model of $hGBP1_F$ function. After binding of GTP to $hGBP1_F$ and release of the farnesyl anchor, $hGBP1_F$ may follow two cycles: membrane binding with further membrane tethering (*Left* cycle) or polymerization by formation of a disk in a first phase accompanied by slow GTP hydrolysis followed by stacking of the circular structures to cylindrical structures enabling faster GTP turnover (*Right* cycle). See the text for more details. (*Inset*) With the subdomains highlighted in different colors, schematic representation of hGBP1 is according to the crystal structure of nonfarnesylated protein in the nucleotide-free state (Protein Data Bank ID code 1DG3). The farnesyl anchor at the C terminus is depicted as a blue zigzag line (ellipse).

contacts established in the cylinder are responsible for the enhanced turnover rate and for the production of GMP, as both rate and product ratio are similar to LG domain dimer activity. Because the transition from the slow to the fast phase of GTP hydrolysis coincides with the appearance of large polymers, which can be detected by turbidity measurements, it is possible that the LG domains of $hGBP1_F$ in the circular structures are not able to form the activating dimer that was observed in the structure of the isolated LG domain (18), unless molecules from adjacent rings come into contact. Intriguingly, the presence of liposomes prevents the shift of the hydrolysis rate toward the fast mode (Fig. 3 *D* and *E*), also decreasing the formation of GMP (Fig. S6*D*). This observation can be rationalized by membrane insertion of $hGBP1_F$ at the expense of polymer formation: as in the phase of building up the circular structures by lateral assembly of $hGBP1_F$, the protein apparently does not form activating LG domain contacts when bound to the membrane surface *in cis*. We have made a similar observation for hGBP1 artificially attached to a chip surface, which also resulted in decreased enzymatic activity (20). Considering a possible GTPase activating effect for hGBP1 dimers *in trans*—dimers bound to different membranes—this effect would be hardly detectable. The contact area between two associated vesicles is too small compared with the total vesicle surface, meaning there is only a small fraction of hGBP1 dimers *in trans* compared with the whole hGBP1 pool.

Recent studies on hGBP1 have reported a granular appearance of hGBP1 within the cell (27), which has also been observed for murine GBP2, an ortholog of hGBP1 (29). It has been suggested that the observed granular distribution of hGBP1 within the cell is based on binding of the protein to vesicular structures. We found hGBP1 partially colocalized with several different markers along the phagolysosomal pathway and in particular to phagosomes induced by latex beads (Figs. S9 and S10). Overexpression of marker proteins such as Rab5, Rab7, or Rab9 enhanced this colocalization. Other groups have already identified certain GBPs on phagocytosed latex bead (42, 43) and bacteria (44, 45). In some cases, we observed recruitment of hGBP1 very early during formation of phagocytic cups. In this context it is noteworthy to mention that a direct interaction between hGBP1 and actin has been recently shown (9). Several other groups have found that GBPs are involved in the control of cell proliferation and motility in both humans and mice by interfering with the integrin pathway (8). Along these lines, a role for hGBP1 in the maintenance of the barrier function of the colonic mucosa has been reported (8).

However, our data revealed that individual hGBP1 molecules are not stably membrane associated within the cell but rather in a constant dynamic exchange with the cytosolic pool. This observation is indicated by the fast recovery of hGBP1 in FRAP experiments on both punctate and phagosomal structures (Fig. 5), which is similar to the fast dynamics of the membrane interaction of hGBP1 we observed in vitro. We assume that at least those punctate structures that colocalize with Rab proteins are indeed vesicles. However, the ability of $hGBP1_F$ to polymerize in vitro, which we report in this study as well, implies that hGBP1 puncta that do not colocalize with phagolysosomal marker proteins could represent polymers of hGBP1. Similar to the current model for Mx proteins and the mitochondrial Drp1, such polymers of hGBP1 could serve as protein depots, ensuring a kind of buffer function for the rapid mobilization of the protein in immune response (46–48). Alternatively, such polymers could function as a scaffold for the assembly of other large immune-related complexes such as the inflammasome (5, 49, 50). At this point, we do not have data to judge the relative amounts of hGBP1 assembled in polymers or residing at membrane surfaces. High intracellular concentrations of hGBP1 are only present after stimulation by IFN-γ or other cytokines. Nevertheless, the enzymatic activity is crucial for polymer formation and at the same time it allows for a highly dynamic assembling process, making hGBP1 molecules available wherever in the cell and whenever they are needed (e.g., parasite combat).

Finally, we report membrane tethering features of $hGBP1_F$, which are also strictly nucleotide controlled (Fig. 4). A number of DLPs are involved in the fusion events within the cell (4, 10, 51). The molecular mechanism of membrane tethering and fusion by dynamin-related GTPases is best understood for atlastins (31, 52). We suggest that $hGBP1_F$ might mediate the tethering effect through dimerization of LG domains similar to atlastins. Our previous results demonstrate the ability of hGBP1 to dimerize through its LG domains in the presence of nonhydrolyzable GTP analogs (11, 18). The observation of the vesicle tethering effect of $hGBP1_F$ in the presence of GTPγS implies that GTP hydrolysis is not required for the tethering activity. However, it is intriguing to see that GTP hydrolysis leads to a much faster increase of the contact area between the two vesicles. Along this line, after consumption of GTP, a relaxation back to a presumably nontensed situation of the two contacting membranes is observed. We did not observe any fusion events of GUVs mediated by $hGBP1_F$, a finding also supported by reversible detachment of tethered LUVs upon GMP addition (Fig. S8). However, membrane fusion may require the aid of other proteins, which was not possible to elucidate with our experimental setup. Nevertheless, the observation of tethering underlines the functional similarity of GBPs with atlastins and also other dynamin family members as recently shown for mitofusin (53). Recent studies on the antibacterial effect of GBPs indicate that hGBP1 and 2 are recruited to bacterial inclusions of *Chlamydia trachomatis* and trigger their rerouting for lysosomal degradation (54). It is tempting to speculate that the tethering effect of hGBP1 and its localization along the phagolysosomal pathway, which we report here, could be the basis for the physiological function of the protein. The tethering of phagolysosomal membranes could result in an enhanced clearance of intracellular pathogens by a more efficient delivery to lysosomes. Similarly, hGBP1 could stimulate the internalization and downregulation of surface receptors, such as certain integrins resulting in the described function in cell adhesion and motility (8). To test these hypotheses, the effect of tethering-impaired mutants of hGBP1 such as R48A could be tested with respect to membrane internalization, vesicular trafficking, and pathogen proliferation.

In conclusion, binding of farnesylated hGBP1 to membranes as well as the formation of hGBP1 polymers are strictly nucleotide controlled. Thus, the farnesyl anchor of hGBP1 is masked in the GDP- and the GMP-bound states, rendering the lipid-modified protein a soluble monomer in solution. As illustrated in our model in Fig. 6, binding of GTP leads to opening of the protein structure and to the release of the farnesyl anchor, enabling its immediate insertion into a membrane in the vicinity of the protein molecule (Fig. 6, *Left* cycle). Alternatively, the opening of hGBP1 and the concomitant availability of the farnesyl group and previously hidden protein surfaces facilitates polymerization of the enzyme, leading first to circular structures expanding to a cylindrical shape by stacking or helix formation in a second phase (Fig. 6, *Right* cycle). Hence, the nucleotide-controlled dynamic process of structural changes and release of the farnesyl anchor can result in membrane insertion followed by tethering processes (or more) on the one hand, and in the formation of well-defined polymers representing enzyme depots on the other.

Molecular switching between different nucleotide states by GTP binding and hydrolysis is the common feature for all GTPases, which is controlled by regulatory proteins. For hGBP1, which does not require any regulatory proteins for nucleotide exchange, we show that this switching controls the availability of the C-terminal farnesyl anchor, which is then used in a dual function, namely, membrane tethering and enzyme polymerization. In hGBP1 the combination of an assembly-stimulated GTPase reaction with a conformation-dependent release of the C-terminal farnesyl anchor in hGBP1 results in a unique molecular machinery—the

farnesyl switch—which controls the membrane recruitment and polymerization activity of the protein.

Methods

Protein Expression, Purification, and Labeling. Synthesis of recombinant hGBP1, either $hGBP1_{NF}$ or $hGBP1_{F}$, was performed as previously described (25). Farnesylated as well as nonfarnesylated proteins were labeled with Alexa-488 C5 maleimide dye (Life Technologies). The reaction mixture was prepared in buffer C (50 mM Tris·HCl, pH 7.9, 5 mM $MgCl_2$, 150 mM NaCl) by mixing 100 μM of protein with 400 μM of dye. After incubation on ice for 60 min, unreacted dye was removed via spin desalting columns (Thermo Scientific).

Preparation of Liposomes. GUVs were electroformed as described before (55) from the mixture of 99% brain polar lipids extract (Avanti Polar Lipids) and 1% tetramethyl rhodamine phosphatidylinositol 4,5-bisphosphate (TMR-PIP_2, Echelon) in 500 mM sucrose solution. LUVs were produced by extrusion through polycarbonate filters with a defined pore size of 0.1 μm, 0.20 μm, or 1 μm (Whatman) as previously described (25). The size of LUVs was confirmed by DLS.

Confocal Microscopy. A newly assembled open homemade observation chamber was incubated with a casein solution (1 mg/mL) for 5 min to prevent adhesion of GUVs to the coverslip. After rinsing the chamber with buffer C (see above), the chamber was filled with 300 μL of experimental mixture prepared in buffer C, followed by injection of GUVs (3 μL). Protein and lipid fluorescence channels were observed by dual-color confocal microscopy ($\lambda_1 = 488$ nm and $\lambda_2 = 543$ nm) on a Nikon Eclipse Ti inverted microscope (Nikon). If required, GUVs were manipulated by micropipettes controlled by a motorized micromanipulator (MP-225, Sutter Instrument). Injection of either protein or nucleotide into the chamber was performed with an injection micropipette having typically a radius of 10 μm, controlled with a hydraulic micromanipulator (Narishige). All experiments were performed with identical laser power and gain settings as well as with the same illumination and detection settings. In dissociation and tethering assays, all experiments were recorded as fluorescent videos in the presence of oxygen scavenging mix [25 mM glucose, 0.37 mg/mL glucose oxidase (Sigma-Aldrich), 0.21 mg/mL catalase (Sigma-Aldrich), 5 mM DTT].

Image Analysis. All fluorescent images were processed and analyzed with ImageJ software. Fluorescence signals of the protein on the membrane of GUVs, $F_{membrane}$ was quantified with the PlotProfile built-in command of ImageJ across narrow equatorial rectangles (Fig. S7 and *SI Methods*). The background fluorescence of unbound protein, $F_{background}$ was measured in the vicinity of GUVs. The fluorescence intensity of the GUV-bound protein was denoted as $I = (F_{membrane} - F_{background})$. For dissociation and tethering assays, fluorescence values of the GUV-bound protein were taken as $F_{membrane}$. For the quantification of the tethering effect, the contact length was defined as a distance between two ends of a membrane segment shared by a pair of GUVs. The contact lengths were quantified from the images by a self-designed algorithm using a javascript for ImageJ (Fig. S7 and *SI Methods*).

Transfections and Fluorescence Microscopy. HeLa B cells (European Collection of Authenticated Cell Cultures 85060701) were grown on coverslips in DMEM supplemented with 10% heat-inactivated calf serum (Sigma-Aldrich), penicillin (100 units/mL) (Gibco), streptomycin (100 mg/mL), and nonessential amino acids solution 10 mM (100×) (Gibco) at 37 °C with 5% CO_2 in a humidified incubator. Expression of hGBP1 was induced with 200 units/mL of recombinant human IFN-γ (PeproTech) for at least 24 h. For transient transfections the GeneJuice reagent (Novagen) was used according to the manufacturer's instructions.

Phagocytosis of latex beads was stimulated by starving in FCS-free DMEM for 2 h before adding of fluorescent or nonfluorescent latex beads (Life Technologies). After another 2 h, cells were either fixed for 20 min in 4% paraformaldehyde in PBS or analyzed by life cell imaging on a Nikon Eclipse Ti spinning disk confocal microscope. Images were analyzed with Volocity (Perkin-Elmer). After taking a reference picture of the unbleached cell, the ROI was bleached with 561-nm or 488-nm lasers with 100% laser power and a duration of 30 cycles (several seconds). Subsequently, cells were continuously imaged for 1 min and during the following 5 min, two pictures per minute were taken. In addition, one ROI of any fluorescent structure within the cell and another outside of the cell were imaged for normalization. Normalized curves were fitted with an exponential function yielding half-lives ($\tau_{1/2}$) of fluorescence recovery.

Absorbance-Based Polymerization Assay. Absorbance-based measurements were performed in quartz precision cells (Hellma Analytics) on Specord200 UV/Vis spectrophotometer (AnalytikJena). The absorbance of the sample was measured at 350 nm in temperature-controlled cuvettes. Nucleotides were injected into the cuvette at final concentrations of 1 mM after initial preequilibration of the experimental mixture for 200 s. Experiments were performed either in buffer C (see above) or in buffer D (50 mM Tris·HCl, pH 8.0, 130 mM KCl, 2 mM $MgCl_2$).

In the presence of GTP, we additionally monitored the nucleotide composition within the experimental mixture if required. For that monitoring, at defined time points, 5-μL samples were taken from the cuvettes and the GTPase reaction was immediately stopped by addition of 10 μL of 10% H_3PO_4, which was followed by neutralization with 30 μL of 0.77 M K_2HPO_4. Final samples were centrifuged for 2 min at 16,000 × *g* and further nucleotide composition was analyzed as described previously (19). Briefly, nucleotides were separated by reversed-phase HPLC using a Chromolith Performance RP-18 endcapped column (Merck) and monitored at 254 nm (MD-2010 Plus, Jasco). For quantifying the share of GMP, GDP, and GTP, peak areas corresponding to each nucleotide were integrated with the manufacturer's software. For experiments in the presence of liposomes, LUVs were produced by extrusion through polycarbonate filters with a defined pore size of 0.1 μm (Whatman) as previously described (25).

Monitoring Polymerization of hGBP1 with Dynamic Light Scattering. Dynamic light scattering of unmodified and farnesylated hGBP1 was determined with the Zetasizer Nano ZS (Malvern Instruments) under different conditions. A total of 20 μM of protein in buffer D (see above) in a UV microcuvette was placed into the cell holder and preincubated at 25 °C for 5 min. The measurement was started quickly after addition of 300 μM $AlCl_3$, 10 mM NaF, and 200 μM GDP (GDP·AlFx) or 1 mM GTP in a total volume of 84 μL. The change of the particle size was monitored over 6–10 measurements, each consisting of four runs of 10 s each and with a delay of 4 s between the measurements. The hydrodynamic radius (R_H) of the particles was determined with the manufacturer's software.

Negative Stain Electron Microscopy. Polymerization of hGBP1 was analyzed by negative stain electron microscopy. Pure protein (10 μM) in buffer D with 2 mM DTT was incubated at room temperature for 5–15 min in the presence of 200 μM GDP with 300 μM $AlCl_3$ and 10 mM NaF or 1 mM GTP or GTPγS, respectively, or in the absence of nucleotide. Samples were bound to a Ni-300 grid with an incubation for 5 min. After removal of excess solution, negative staining was done two times for 2 min each with 2% uranyl acetate. Finally, preparations were examined in a Zeiss EM109 microscope (Zeiss).

ACKNOWLEDGMENTS. We thank Klaus Boller and Regina Eberle for help with electron microscopy and Christiane Horst and Claudia Grundmann for excellent technical support. The research leading to these results has received funding from the European Commission's Seventh Framework Program (FP7/2007-2013) under Grant TRANSPOL 264399; and the Deutsche Forschungsgemeinschaft with Grants HE 2679/6-1, PR 1090/3-1 within the priority program 1580, within the collaborative research center SFB635 and within the Cluster of Excellence RESOLV, EXC 1069.

1. Cheng YS, Colonno RJ, Yin FH (1983) Interferon induction of fibroblast proteins with guanylate binding activity. *J Biol Chem* 258:7746–7750.
2. Praefcke GJK, McMahon HT (2004) The dynamin superfamily: Universal membrane tubulation and fission molecules? *Nat Rev Mol Cell Biol* 5:133–147.
3. Ferguson SM, De Camilli P (2012) Dynamin, a membrane-remodelling GTPase. *Nat Rev Mol Cell Biol* 13:75–88.
4. McNew JA, Sondermann H, Lee T, Stern M, Brandizzi F (2013) GTP-dependent membrane fusion. *Annu Rev Cell Dev Biol* 29:529–550.
5. Pilla-Moffett D, Barber MF, Taylor GA, Coers J (2016) Interferon-inducible GTPases in host resistance, inflammation and disease. *J Mol Biol* 428:3495–3513.
6. Meunier E, Broz P (2016) Interferon-inducible GTPases in cell autonomous and innate immunity. *Cell Microbiol* 18:168–180.
7. Man SM, Karki R, Kanneganti T-D (2017) Molecular mechanisms and functions of pyroptosis, inflammatory caspases and inflammasomes in infectious diseases. *Immunol Rev* 277:61–75.
8. Britzen-Laurent N, Herrmann C, Naschberger E, Croner RS, Stürzl M (2016) Pathophysiological role of guanylate-binding proteins in gastrointestinal diseases. *World J Gastroenterol* 22:6434–6443.
9. Ostler N, et al. (2014) Gamma interferon-induced guanylate binding protein 1 is a novel actin cytoskeleton remodeling factor. *Mol Cell Biol* 34:196–209.
10. Daumke O, Praefcke GJK (2016) Invited review: Mechanisms of GTP hydrolysis and conformational transitions in the dynamin superfamily. *Biopolymers* 105:580–593.
11. Prakash B, Praefcke GJK, Renault L, Wittinghofer A, Herrmann C (2000) Structure of human guanylate-binding protein 1 representing a unique class of GTP-binding proteins. *Nature* 403:567–571.

12. Vöpel T, et al. (2010) Mechanism of GTPase-activity-induced self-assembly of human guanylate binding protein 1. *J Mol Biol* 400:63–70.
13. Vöpel T, Kunzelmann S, Herrmann C (2009) Nucleotide dependent cysteine reactivity of hGBP1 uncovers a domain movement during GTP hydrolysis. *FEBS Lett* 583: 1923–1927.
14. Vöpel T, et al. (2014) Triphosphate induced dimerization of human guanylate binding protein 1 involves association of the C-terminal helices: A joint double electron-electron resonance and FRET study. *Biochemistry* 53:4590–4600.
15. Schwemmle M, Staeheli P (1994) The interferon-induced 67-kDa guanylate-binding protein (hGBP1) is a GTPase that converts GTP to GMP. *J Biol Chem* 269:11299–11305.
16. Kunzelmann S, Praefcke GJK, Herrmann C (2006) Transient kinetic investigation of GTP hydrolysis catalyzed by interferon-gamma-induced hGBP1 (human guanylate binding protein 1). *J Biol Chem* 281:28627–28635.
17. Praefcke GJK, Geyer M, Schwemmle M, Robert Kalbitzer H, Herrmann C (1999) Nucleotide-binding characteristics of human guanylate-binding protein 1 (hGBP1) and identification of the third GTP-binding motif. *J Mol Biol* 292:321–332.
18. Ghosh A, Praefcke GJK, Renault L, Wittinghofer A, Herrmann C (2006) How guanylate-binding proteins achieve assembly-stimulated processive cleavage of GTP to GMP. *Nature* 440:101–104.
19. Kunzelmann S, Praefcke GJK, Herrmann C (2005) Nucleotide binding and self-stimulated GTPase activity of human guanylate-binding protein 1 (hGBP1). *Methods Enzymol* 404: 512–527.
20. Syguda A, et al. (2012) Immobilization of biotinylated hGBP1 in a defined orientation on surfaces is crucial for uniform interaction with analyte proteins and catalytic activity. *Langmuir* 28:6411–6418.
21. Abdullah N, Balakumari M, Sau AK (2010) Dimerization and its role in GMP formation by human guanylate binding proteins. *Biophys J* 99:2235–2244.
22. Olszewski MA, Gray J, Vestal DJ (2006) In silico genomic analysis of the human and murine guanylate-binding protein (GBP) gene clusters. *J Interferon Cytokine Res* 26: 328–352.
23. Stickney JT, Buss JE (2000) Murine guanylate-binding protein: Incomplete geranylgeranyl isoprenoid modification of an interferon-gamma-inducible guanosine triphosphate-binding protein. *Mol Biol Cell* 11:2191–2200.
24. Nantais DE, Schwemmle M, Stickney JT, Vestal DJ, Buss JE (1996) Prenylation of an interferon-gamma-induced GTP-binding protein: The human guanylate binding protein, huGBP1. *J Leukoc Biol* 60:423–431.
25. Fres JM, Müller S, Praefcke GJK (2010) Purification of the CaaX-modified, dynamin-related large GTPase hGBP1 by coexpression with farnesyltransferase. *J Lipid Res* 51: 2454–2459.
26. Tripal P, et al. (2007) Unique features of different members of the human guanylate-binding protein family. *J Interferon Cytokine Res* 27:44–52.
27. Britzen-Laurent N, et al. (2010) Intracellular trafficking of guanylate-binding proteins is regulated by heterodimerization in a hierarchical manner. *PLoS One* 5:e14246.
28. Modiano N, Lu YE, Cresswell P (2005) Golgi targeting of human guanylate-binding protein-1 requires nucleotide binding, isoprenylation, and an IFN-gamma-inducible cofactor. *Proc Natl Acad Sci USA* 102:8680–8685.
29. Kravets E, et al. (2012) The GTPase activity of murine guanylate-binding protein 2 (mGBP2) controls the intracellular localization and recruitment to the parasitophorous vacuole of Toxoplasma gondii. *J Biol Chem* 287:27452–27466.
30. Praefcke GJK, et al. (2004) Identification of residues in the human guanylate-binding protein 1 critical for nucleotide binding and cooperative GTP hydrolysis. *J Mol Biol* 344:257–269.
31. Liu TY, et al. (2015) Cis and trans interactions between atlastin molecules during membrane fusion. *Proc Natl Acad Sci USA* 112:E1851–E1860.
32. Jordens I, et al. (2001) The Rab7 effector protein RILP controls lysosomal transport by inducing the recruitment of dynein-dynactin motors. *Curr Biol* 11:1680–1685.
33. Kravets E, et al. (2016) Guanylate binding proteins (GBPs) directly attack *T. gondii* via supramolecular complexes. *eLife* 5:1–30.
34. Schmick M, Kraemer A, Bastiaens PIH (2015) Ras moves to stay in place. *Trends Cell Biol* 25:190–197.
35. Goody RS, Rak A, Alexandrov K (2005) The structural and mechanistic basis for recycling of Rab proteins between membrane compartments. *Cell Mol Life Sci* 62: 1657–1670.
36. Pasqualato S, Renault L, Cherfils J (2002) Arf, Arl, Arp and Sar proteins: A family of GTP-binding proteins with a structural device for 'front-back' communication. *EMBO Rep* 3:1035–1041.
37. Uthaiah RC, Praefcke GJK, Howard JC, Herrmann C (2003) IIGP1, an interferon-gamma-inducible 47-kDa GTPase of the mouse, showing cooperative enzymatic activity and GTP-dependent multimerization. *J Biol Chem* 278:29336–29343.
38. Hinshaw JE, Schmid SL (1995) Dynamin self-assembles into rings suggesting a mechanism for coated vesicle budding. *Nature* 374:190–192.
39. Klockow B, et al. (2002) The dynamin A ring complex: Molecular organization and nucleotide-dependent conformational changes. *EMBO J* 21:240–250.
40. Haller O, Kochs G (2002) Interferon-induced mx proteins: dynamin-like GTPases with antiviral activity. *Traffic* 3:710–717.
41. Low HH, Löwe J (2006) A bacterial dynamin-like protein. *Nature* 444:766–769.
42. Jutras I, et al. (2008) Modulation of the phagosome proteome by interferon-gamma. *Mol Cell Proteomics* 7:697–715.
43. Trost M, et al. (2009) The phagosomal proteome in interferon-gamma-activated macrophages. *Immunity* 30:143–154.
44. Tietzel I, El-Haibi C, Carabeo RA (2009) Human guanylate binding proteins potentiate the anti-chlamydia effects of interferon-gamma. *PLoS One* 4:e6499.
45. Fiegl D, et al. (2013) Amphisomal route of MHC class I cross-presentation in bacteria-infected dendritic cells. *J Immunol* 190:2791–2806.
46. Patzina C, Haller O, Kochs G (2014) Structural requirements for the antiviral activity of the human MxA protein against Thogoto and influenza A virus. *J Biol Chem* 289: 6020–6027.
47. Gao S, et al. (2011) Structure of myxovirus resistance protein a reveals intra- and intermolecular domain interactions required for the antiviral function. *Immunity* 35: 514–525.
48. Macdonald PJ, et al. (2014) A dimeric equilibrium intermediate nucleates Drp1 reassembly on mitochondrial membranes for fission. *Mol Biol Cell* 25:1905–1915.
49. Shenoy AR, et al. (2012) GBP5 promotes NLRP3 inflammasome assembly and immunity in mammals. *Science* 336:481–485.
50. Finethy R, et al. (2015) Guanylate binding proteins enable rapid activation of canonical and noncanonical inflammasomes in Chlamydia-infected macrophages. *Infect Immun* 83:4740–4749.
51. Escobar-Henriques M, Anton F (2013) Mechanistic perspective of mitochondrial fusion: Tubulation vs. fragmentation. *Biochim Biophys Acta* 1833:162–175.
52. Hu J, Rapoport TA (2016) Fusion of the endoplasmic reticulum by membrane-bound GTPases. *Semin Cell Dev Biol* 60:105–111.
53. Qi Y, et al. (2016) Structures of human mitofusin 1 provide insight into mitochondrial tethering. *J Cell Biol* 215:621–629.
54. Al-Zeer MA, Al-Younes HM, Lauster D, Abu Lubad M, Meyer TF (2013) Autophagy restricts Chlamydia trachomatis growth in human macrophages via IFNG-inducible guanylate binding proteins. *Autophagy* 9:50–62.
55. Morlot S, et al. (2012) Membrane shape at the edge of the dynamin helix sets location and duration of the fission reaction. *Cell* 151:619–629.